

# Constraining the star formation rate with the extragalactic background light

A. A. Korochkin<sup>1,2</sup><sup>★</sup>, G. I. Rubtsov<sup>1</sup>

<sup>1</sup> *Institute for Nuclear Research of the Russian Academy of Sciences, 60th October Anniversary st. 7a, 117312, Moscow, Russia*

<sup>2</sup> *Faculty of Physics, M V Lomonosov Moscow State University, Vorobyovy Gory, 1-2, Moscow, 119991, Russia*

Accepted XXX. Received YYY; in original form ZZZ

## ABSTRACT

The present day spectrum of the extragalactic background light (EBL) in UV, optical and IR wavelengths is the integral result of multiple astrophysical processes going on throughout the evolution of the Universe. The relevant processes include star formation, stellar evolution, light absorption and emission by the cosmic dust. The properties of these processes are known with uncertainties which contribute to the EBL spectrum precision. In the present paper we develop a numerical model of the EBL spectrum while maintaining the explicit dependence on the astrophysical parameters involved. We constructed a Markov Chain in the parameter space by using the likelihood function built with the up-to-date upper and lower bounds on the EBL intensity. The posterior distributions built with the Markov Chain Monte Carlo method are used to determine an allowed range of the individual parameters of the model. Consequently, the star formation rate multiplication factor is constrained in the range  $1.01 < C_{\text{sfr}} < 1.69$  at 68% C.L. The method also results in the bounds on the lifetime, radius, dust particle density and opacity of the molecular clouds that have large ambiguity otherwise. It is shown that there is a reasonable agreement between the model and the intensity bounds while the astrophysical parameters of the best fit model are close to their estimates from literature.

**Key words:** galaxies: star formation – galaxies: fundamental parameters

## 1 INTRODUCTION

Extragalactic background light (EBL) is a radiation emitted by stars and cosmic dust throughout the whole lifetime of the Universe at ultraviolet, optical and infrared wavelengths. In ultraviolet and optical spectral region it is dominated by the star radiation while the infrared spectrum is determined by emission of the dust. The understanding of the EBL is an attractive task for several reasons. First, the origin of EBL is directly connected to the star formation history and may shed a light on the details of the evolution of the Universe. Second, EBL is a key element in multiple physical processes in the intergalactic space. One of these processes is the attenuation of the high energy gamma-rays by the pair production on background photons [Nikishov \(1962\)](#). Given a photon with the TeV energy, the pair production cross-section has a maximum for infrared photons, which constitute an appreciable part of the total flux of EBL. Therefore, an accurate knowledge of the EBL spectrum is important for reconstruction of the intrinsic spectra and understand-

ing the emission mechanism of the distant blazars [Gilmore et al. \(2012\)](#), [Franceschini & Rodighiero \(2017\)](#).

Finally, recent studies report anomalies in the reconstructed spectra of the distant blazars. As was shown in [Horns & Meyer \(2012\)](#); [Rubtsov & Troitsky \(2014\)](#), the application of the most conservative EBL models results in the upward breaks in the intrinsic spectra which are unlikely to be explained by the source-intrinsic features. The position of the break corresponds to the energy at which an attenuation becomes significant and the magnitude of the break is stronger for more distant sources. The spectra of the blazars will be free from artificial features if the real density of the EBL flux is at least twice weaker than one in the most conservative models. The discussion of the possibility of such a significant reduction required a detailed analysis of the physical factors accounting for EBL formation. The alternative explanations of the anomalous transparency of the Universe include new physics with the hypothetical axion-like particles, see [Troitsky \(2017\)](#), [De Angelis et al. \(2007\)](#), [Simet et al. \(2008\)](#), [Fairbairn et al. \(2011\)](#) for a review and new astrophysics [Essey & Kusenko \(2010\)](#), [Dzhatdoev et al. \(2017\)](#). In the latter class of models it is assumed that addi-

<sup>★</sup> E-mail:aa.korochkin@physics.msu.ru

tional high-energy gamma-rays are produced as the secondaries in the cascades, initiated by the gamma-rays or the ultra-high-energy protons emitted at the same sources.

The estimation of the EBL is a complex problem for which several approaches both experimental and computational have been developed. First, a large group of methods is based on the observations. A direct observation of EBL is a challenging experimental problem because of the dominant contribution of the Zodiacal light and emission of the Galaxy in the same spectral region. For this reason, these methods in turn may be split into the two categories. In the first case unwanted contribution is avoided using the galaxy count method. The method relies on the deep field observation of the galaxy and the EBL is estimated as the sum of the fluxes of the discrete sources [Keenan et al. \(2010\)](#), [Madau & Pozzetti \(2000\)](#). As it follows from description this approach can only estimate the lower limit of EBL due to possible undercount of the galaxies beyond the sensitivity level of the instrument or underestimation of the faintest areas of the objects detected [Bernstein \(2007\)](#). Another way to make measurement free of the Zodiacal and Galaxy light corrections is to invoke special techniques to subtract the background contributions. That results in EBL considerably higher than that inferred from galaxy count method [Matsuura et al. \(2017\)](#), [Mattila et al. \(2017\)](#).

Another large group of approaches is based on the numerical calculation of the EBL. These methods differ by the basic assumptions made and may be divided into several subgroups. The first category is based on the evolution in time of the galaxy properties. Such an evolution may be obtained either by direct observations of galaxy evolution or indirectly estimated according to some prescription. This method was used in some of the first models of the EBL [Madau et al. \(1998\)](#), [Pei et al. \(1999\)](#), [Kneiske et al. \(2002\)](#), [Kneiske et al. \(2004\)](#) and it is still relevant due to the recent large-scale surveys at ultraviolet and infrared wavelengths [Finke et al. \(2010\)](#). Another category of approaches uses a backward evolution of the present day galaxy emissivity according to a given prescription and accounts for the change of the star formation rate and other redshift dependent factors [Franceschini & Rodighiero \(2017\)](#), [Franceschini et al. \(2001\)](#), [Rowan-Robinson \(2001\)](#), [Franceschini et al. \(2008\)](#), [Dominguez et al. \(2011\)](#), [Stecker et al. \(2016\)](#).

The last scenario for treating EBL is so called the forward evolution approach. This is the most fundamental and challenging way of calculation. It starts with the very basic assumptions about the Universe and its structure formation. Often the structure formation process is based on semi-analytic models of cold dark matter merger trees [Primack et al. \(1999\)](#), [Gilmore et al. \(2012\)](#). Being the most complete, the method allows to pinpoint the physical reasons for time-dependence of the EBL.

In this Paper we follow the second scenario and present a numerical model of the EBL built upon the dynamics of the star formation and the evolution of stars. Our goal is to build a model with the explicit dependence on the underlying astrophysical parameters. The analytic part of the model is explained in Section 2 and the numerical part is presented as a publicly-available code<sup>1</sup>, see Appendix A. The model al-

lows to explore the parameter space with the Markov Chain Monte Carlo (MCMC) method. For this purpose in Section 3 we build a likelihood function for the EBL spectrum using the modern upper and lower constrains at multiple wavelengths. The resulting marginal posterior distributions for the parameters involved are given in Section 4. It is shown that several parameters, including the multiplication factor of the star formation rate and the lifetime, radius, dust particle density and opacity of the molecular clouds of the molecular clouds are solidly constrained by the EBL observations. The results are summarized in 5.

## 2 MODEL

Our goal is to build the empirical model of the formation and evolution of stars and galaxies. The model we plan to construct will be then directly translated into the EBL spectrum. It's unavoidable for the model to be dependent on a number of astrophysical parameters, which are known with a limited precision. We will keep these dependencies explicit, so the parameter space may be further probed with the MCMC technique.

At first the contribution of stars to the EBL will be described, and then the absorption and re-emission of light by dust will be taken into account. We use the standard  $\Lambda$ CDM cosmological model to derive the functional dependencies between comoving distance  $r$ , redshift  $z$  and time  $t$ .

$$r(z) = \frac{c}{H_0} \int_0^z \frac{dz}{\sqrt{\Omega_m(1+z)^3 + \Omega_\Lambda}} \quad (1)$$

$$z(t) = \left(\frac{\Omega_\Lambda}{\Omega_m}\right)^{\frac{1}{3}} \left[ \sinh\left(\frac{3}{2}\Omega_\Lambda^{\frac{1}{2}}tH_0\right) \right]^{-\frac{2}{3}} - 1, \quad (2)$$

where the Hubble constant  $H_0 = 67.8$  km/s/Mpc, the matter density parameter  $\Omega_m = 0.309$ , the dark energy density parameter  $\Omega_\Lambda = 0.691$  and  $c$  is the speed of light. The parameters of the cosmological model are measured within the high accuracy [Ade et al. \(2016\)](#) and therefore are considered fixed for the purposes of the present study. We assume Chabrier initial mass function (IMF) to describe mass distribution of newborn stars [Chabrier \(2003\)](#). Following [Gilmore et al. \(2012\)](#) we assume that the IMF doesn't depend on the redshift:

$$\xi(m) = \begin{cases} \frac{C_{\text{imf}}}{m} e^{-\frac{(\log(m) - \log(m_0))^2}{2D}} & \text{if } m \leq 1, \\ km^{-a_{\text{imf}}} & \text{if } m > 1. \end{cases} \quad (3)$$

Masses of stars are measured in the units of the Solar mass. The parameters  $m_0$ ,  $D$  and  $a$  will undergo variations while  $C_{\text{imf}}$  and  $k$  are determined from normalization and continuity. The initial mass function is bounded from below by the minimal mass  $m_{\text{min}} = 0.08$ . If the mass of the star is less than  $m_{\text{min}}$  then the hydrogen thermonuclear fusion reactions in the core will not ignite. The upper bound of the mass distribution  $m_{\text{max}}$  is another free parameter of the model. The initial values for the variable parameters of the IMF are:  $m_0 = 0.079$ ,  $D = 0.69$ ,  $a = 2.3$  and  $m_{\text{max}} = 100$ . For the sake

<sup>1</sup> <https://github.com/Semk0/EBL-model>

of convenience we will use mass normalization of the IMF:

$$\int_{m_{\min}}^{m_{\max}} m\xi(m)dm = 1 \quad (4)$$

The mass of stars, born at redshift  $z$  per unit time per unit volume is described by the star formation rate (SFR)  $\psi(z)$ . Here we will use SFR, obtained in Gilmore et al. (2012). We parametrize the SFR with a single multiplication factor  $C_{\text{sfr}}$  with initial value equal to unity.

To determine the spectrum of the star with the mass  $m$  at the age  $\eta$  near the surface of this star we use stellar evolution tracks calculated by Hurley et al. Hurley et al. (2000), which give us radius  $R$ , temperature  $T$  and lifetime  $\eta_{\text{life}}$  dependence on age. Let's define this spectrum as  $B(\lambda, m, \eta, z = 0)$  there the last argument is reserved for the redshift.

$$B_s(\lambda, m, \eta, 0) = \frac{2\pi hc^2}{\lambda^5} \frac{1}{e^{\frac{hc}{kT(m, \eta)\lambda}} - 1} \quad (5)$$

If we consider the star at the distance  $r$  from the detector, the registered emission will be different from (5), due to geometric dilution and cosmological redshift. The time  $\eta$  now will denote the age of the star at the moment of the emission of radiation registered today. To calculate new spectrum we use a standard trick: replace  $\lambda$  by  $\frac{\lambda}{1+z}$  and divide the full expression by  $(1+z)^3$ . First  $(1+z)$  is responsible for decreasing the energy of the photons, second is responsible for decreasing the number of registered photons per unit time and the last is responsible for broadening of the spectrum. Also the expression must be multiplied by the geometrical factor  $\left(\frac{R(\eta)}{r(z)}\right)^2$ :

$$B_s(\lambda, m, \eta, z) = \left(\frac{R(m, \eta)}{r(z)}\right)^2 (1+z)^{-3} B\left(\frac{\lambda}{1+z}, m, \eta, z = 0\right) \quad (6)$$

Distance  $r(z)$  is calculated by (1).

Using the above definitions one may write an expression to determine the spectrum of a galaxy of age  $\eta_g$  and redshift  $z_g$ . Moreover, we assume that the star formation began in all galaxies simultaneously at time  $t_i$ . The light emitted at time  $t_i$  is now registered with the redshift  $z_i = z(t_i)$ . Then the galaxy age  $\eta_g$  and redshift  $z_g$  are related with the expression:

$$\eta_g = t(z_g) - t(z_i) \quad (7)$$

The function  $t(z)$  is the inverse of (2). Thus we obtain for galaxy spectrum:

$$G_s(\lambda, z_g) = \int_{m_{\min}}^{m_{\max}} dm \int_0^{\eta_{\text{end}}(m)} d\eta' B_s(\lambda, m, \eta', z_g) \xi(m) \psi(t(z_g) - \eta') \quad (8)$$

Upper limit  $\eta_{\text{end}}$  in time integral depends on the mass and determined by

$$\eta_{\text{end}}(m) = \min(\eta_g, \eta_{\text{life}}(m)) \quad (9)$$

On the other hand the presence of dust and absorbers in the galaxies and interstellar medium should be taken into account. Following Charlot & Fall (2000) we assume, that the star formation took place only in the giant molecular

clouds which will cover the newborn stars with the shell of dust and gas. Dust grains consist mostly of graphite and silicate, so they have non-zero absorption coefficients at visible and ultraviolet wavelengths. Thus they will be heated by the newborn stars and re-emit in the infrared part of the spectrum.

Let us now specify the dust model. According to Charlot & Fall (2000) we assume that the birth clouds have finite lifetimes  $\eta_c$ . The parameters of the cloud such as particle number densities and outer radius  $R_c$  stay constant throughout its life, whereas the temperature of different components may change due to evolution of the stars in the center. Moreover, we assume for simplicity that dust has constant particle number density through the entire cloud which is defined by the parameter  $n_d$ . We do not account for the other features of the internal structure of the cloud and following Charlot & Fall (2000) the optical depth will be treated as a free parameter with the two characteristics. First one is the normalization, which corresponds to the optical depth at wavelength  $\lambda_0 = 5500 \text{ \AA}$  and the second is a spectral slope  $n$ . Thence, optical depth at the arbitrary wavelength is determined by

$$\tau(\lambda) = \tau_{\lambda_0} \left(\frac{\lambda}{\lambda_0}\right)^{-n} \quad (10)$$

We assume that the star formation occurs in the center of the birth cloud, so there exists such a value  $\rho \ll R_c$  that all newborn stars are located in the imaginary sphere  $S^{\text{in}}$  with radius  $\rho$ . First of all we calculate spectrum  $B_c(\lambda, \eta, \rho)$  of the newborn stars at the age  $\eta$  on the boundary of the sphere  $S^{\text{in}}$ . On this step we neglect absorption and dependence on redshift:

$$B_c(\lambda, \eta, \rho) = \int_{m_{\min}}^{m_{\max}} dm \int_0^{\eta_{\text{cend}}(m)} d\eta' \left(\frac{R(\eta')}{\rho}\right)^2 \times B(\lambda, m, \eta', z = 0) \xi(m) \psi_c(\eta') \quad (11)$$

where  $\eta_{\text{cend}}(m) = \min(\eta_c, \eta_g, \eta_{\text{life}}(m))$  by analogy with (9) and  $\psi_c(\eta)$  denotes mass of the matter converted into stars in the cloud at the age  $\eta$  per unit time. The total mass of the gas converted into stars throughout life of the cloud  $M_0$  is given by:

$$\int_0^{\eta_c} \psi_c(\eta') d\eta' = M_0 \quad (12)$$

For the sake of simplicity suppose that  $\psi_c(\eta)$  stays constant in time so that:

$$\psi_c = \frac{M_0}{\eta_c} \quad (13)$$

On the other hand,  $\psi_c$  directly proportional to  $\psi(t)$  with the coefficient  $n_{cl}(t)$  which denotes the number of clouds per unit volume.

$$n_{cl}(t) = \frac{\psi(t)}{\psi_c} = \frac{\psi(t)\eta_c}{M_0} \quad (14)$$

Equation (14) will be used for calculating the spectrum of newborn stars in the galaxy. Applying (10) we estimate the absorption for light propagating from  $\rho$  to  $r$ .

$$B_c(\lambda, \eta, r) = \left(\frac{\rho}{r}\right)^2 e^{-\tau_{\lambda_0} \left(\frac{\lambda}{\lambda_0}\right)^{-n}} B_c(\lambda, \eta, \rho) \quad (15)$$

where we again neglected the redshift. Thus  $B_c(\lambda, \eta, R_c)$  denotes contribution of the stars to the spectrum of the cloud calculated on the cloud's boundary. The full spectrum of the cloud contains an additional contribution of dust. Now we describe the assumptions regarding properties of dust. Following [Martinez-Galarza et al. \(2009\)](#) the dust grains are spherical with sizes  $a$  distributed by the power law:

$$dn(a, a + da) = C_d a^{-n_{\text{dust}}} da \quad (16)$$

Initial value for the slope of distribution  $n_{\text{dust}} = 3.5$ . As the sizes of grains are constrained, distribution should be truncated with minimal grain size  $a_{\text{min}}$  and maximal  $a_{\text{max}}$ . We will start setting  $a_{\text{min}} = 5$  nm and  $a_{\text{max}} = 500$  nm. As mentioned above the dust particle number density is constant and allows us to determine normalization constant  $C_d$ .

$$C_d = \frac{(n_{\text{dust}} - 1)n_d}{a_{\text{min}}^{-n_{\text{dust}}+1} - a_{\text{max}}^{-n_{\text{dust}}+1}} \quad (17)$$

Equilibrium temperature  $T_d(a, r)$  of dust grain of size  $a$  at the distance of  $r$  may be found from the energy balance equation:

$$\pi a^2 \int_0^\infty Q_{\text{abs}}^a(\lambda) B_c(\lambda, \eta, r) d\lambda = 4\pi a^2 \int_0^\infty Q_{\text{abs}}^a(\lambda) B_{\text{Pl}}(\lambda, T_d(a, r, \eta)) \quad (18)$$

where emissivity and absorptivity coefficient of grains with size  $a$  are equal due to Kirchoff's law and denoted as  $Q_{\text{abs}}^a(\lambda)$ .  $B_{\text{Pl}}(\lambda, T_d(a, r, \eta))$  is the Planck's law of emissivity.

To find out the full contribution of dust we should integrate over the grain size and over the distance  $r$ . Thus we obtain final formula for calculating dust spectrum:

$$B_d(\lambda, \eta) = \int_{\rho}^{R_{\text{out}}} dr 4\pi r^2 \times \int_{a_{\text{min}}}^{a_{\text{max}}} da \left(\frac{a}{R_{\text{out}}}\right)^2 C_d a^{-n_{\text{dust}}} Q_{\text{abs}}^a(\lambda) B_{\text{Pl}}(\lambda, T_d(a, r, \eta)) \quad (19)$$

In the mid-infrared the principal contribution comes from the polycyclic aromatic hydrocarbons (PAH) molecules, which absorb the starlight producing the spectral lines. The corresponding cross-sections  $\sigma$ , damping constants  $\gamma$ , and cutoff energies  $\lambda_c$  assuming Lorentzian spectral shape are well known and may be found, for example, in [Krugel \(2003\)](#). The PAH spectra is calculated as follows:

$$B_{\text{PAH}}(\lambda, \eta) = \int_{\rho}^{R_{\text{out}}} dr 4\pi r^2 \times n_{\text{PAH}} \int_{\lambda_c}^{\infty} d\lambda' B_c(\lambda', \eta, r) \times \sum_i \left( \sigma_i \frac{\gamma_i c^3 / \lambda^4}{\pi^2 \left( \frac{c^2}{\lambda^2} - \frac{c^2}{\lambda_0^2} \right)^2 + \left( \frac{\gamma_i c}{2\lambda} \right)^2} \right) \quad (20)$$

where  $n_{\text{PAH}}$  is the particle number density of homogeneously distributed PAH molecules, and summing goes over the full set of resonances.

Summarizing the above the full spectrum of the galaxy

with redshift  $z_g$  is expressed as:

$$G(\lambda, z_g) = G_s(\lambda, z_g) + G_c(\lambda, z_g) \quad (21)$$

where:

$$G_s(\lambda, z_g) = \int_{m_{\text{min}}}^{m_{\text{max}}} dm \int_0^{\eta_{\text{end}}(m)} d\eta' B_s(\lambda, m, \eta', z_g) \xi(m) \psi(t(z_g) - \eta') \quad (22)$$

$$\eta_{\text{end}}(m) = \text{Max}(\text{Min}(\eta_g, \eta_{\text{life}}(m) - \eta_c), 0) \quad (23)$$

$$G_c(\lambda, z_g) = \int_0^{\eta_c} d\eta' (B_d(\lambda, \eta', z_g) + B_{\text{PAH}}(\lambda, \eta', z_g) + B_c(\lambda, \eta', R_{\text{out}}, z_g)) \frac{\eta_c}{M_0} \psi(t(z_g) - \eta') \quad (24)$$

Finally, the spectrum of the whole Universe is obtained by integration over the distance, taking into account Calzetti's attenuation law  $C_{\text{calz}}(\lambda)$  for diffuse dust component [Calzetti et al. \(2000\)](#).

$$U(\lambda) = \int_0^{r(z_i)} dr 4\pi r^2 C_{\text{calz}}(\lambda) G(\lambda, z_g(r)) \quad (25)$$

### 3 METHOD

The model of the Section 2 keeps an explicit dependence on a number of parameters. The preferred values and confidence ranges for the parameters will be calculated using the Markov Chain Monte Carlo method. The Markov Chain is constructed with the Metropolis algorithm with the standard likelihood function

$$\mathcal{L} = \prod_i e^{-\frac{(y - y_i)^2}{2\sigma_i^2}}, \quad (26)$$

where  $y_i$  and  $\sigma_i$  are the values and errors of the experimental points. The one-sided limits are included in the product only if  $y > y_i$  for lower limits and if  $y < y_i$  for upper ones.

The likelihood is based on the three categories of the data points which are the lower and upper limits of the EBL and direct measurements. The lower EBL limits usually come from the galaxy count method and provide strict constraints, see Table 2. The upper limits appear either from the direct measurements at the wavelengths where contribution of the Zodiacal light is significant or from the direct measurements combined with some special technique to subtract the excess, see Table 3. We do not include here the constraints from the gamma-ray observations due to possible uncertainties in AGN's spectra. For the wavelengths longer than  $200\mu\text{m}$  the direct measurements are used as it is believed that Zodiacal light contribution is neglectful. We have also added Pioneer 10/11 results because their measurements were conducted far from the region of the potential Solar system background affects, see Table 4.

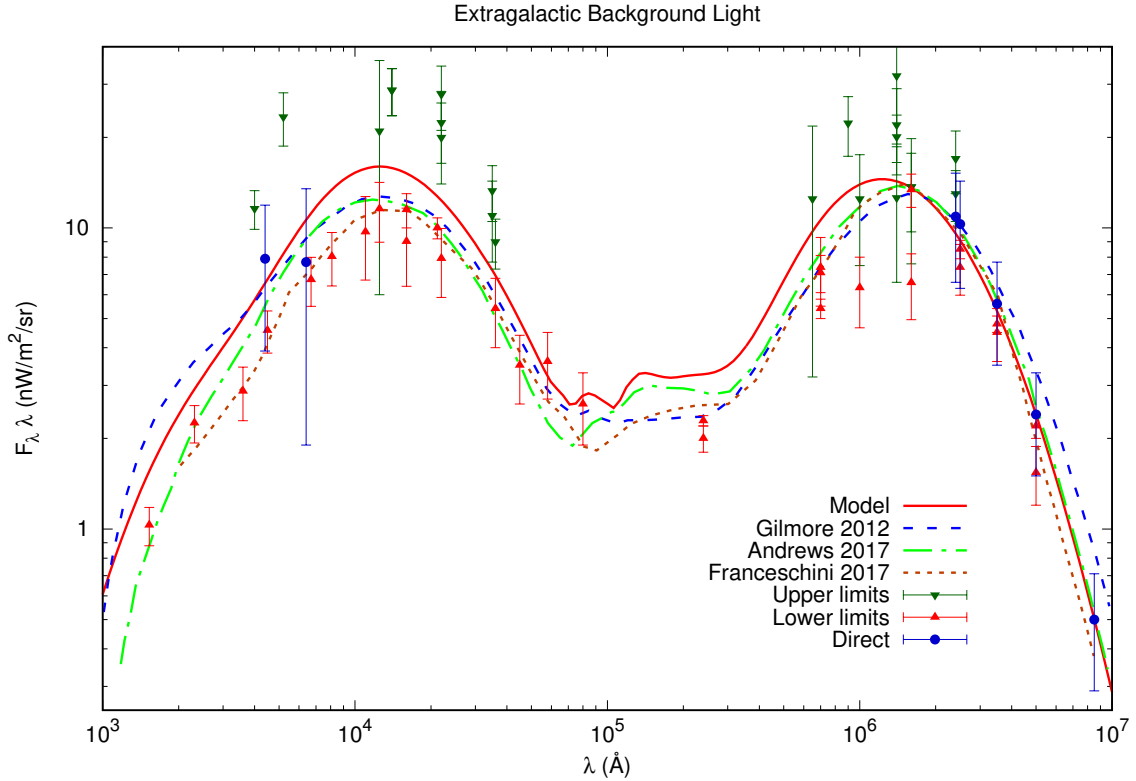


**Figure 1.** Extragalactic background light spectrum. Red line is our best fit result. Blue line is for Gilmore et al. Gilmore et al. (2012) semi-analytic model. Green and brown lines are for Andrews et al. Andrews et al. (2017) and Franceschini et al. Franceschini & Rodighiero (2017) correspondingly. Upward and downward pointing arrows indicate lower and upper EBL limits, see Table 2 and Table ??, circles is for direct measurements, Table ??.

## 4 RESULTS

The Markov chain is built as described at Section 3. Each step of the chain requires to repeat the full calculation of the EBL, so we employ the parallel implementation of the code with `OpenMP`. The chain of the length 42000 is constructed and made available at the <sup>2</sup>.

Given the model and the chain, we begin with proving the consistency of the model and then discuss possible systematics. The EBL spectrum with the best likelihood set of the parameters is shown in Figure 1. The parameters inferred from the MCMC are in a good agreement with the commonly used values, see Table 1. Spectrum demonstrates good accordance in ultraviolet, optical and far infrared bands with the popular models Gilmore et al. (2012) and Franceschini et al. (2008).

We do not account for the AGN's contribution because it is sub-dominant and moreover is subject to large uncertainty Andrews et al. (2017). This contribution may modify the result considerably for  $\lambda < 0.4\mu\text{m}$  and therefore we didn't

account for the experimental points in this range. Another assumption of the model is that all the cloud's parameters are equal. This means that all the diversity of the star forming objects is reduced to only one type of the clouds. We believe this is enough to grasp the main behaviour of these objects.

Let us now describe the outcomes of the main part of the research. All the parameters are divided into four group according to the way they are treated. First group contains the parameters of Chabrier Initial Mass Function namely  $m_0$ ,  $D$ ,  $a_{\text{imf}}$ . They are already limited in Chabrier (2003) so we set the existing confidence intervals as an available freedom for each parameter. The calculations show that the EBL is insensitive to  $m_0$  and  $D$ , while it depends strongly on  $a_{\text{imf}}$ . The resulting value is  $a_{\text{imf}} = 2.29^{+0.15}_{-0.24}$  which is more narrow than the limits from Chabrier (2003). The parameter  $a_{\text{imf}}$  governs the number of massive stars thus this result indicates that the massive stars play an important role in the EBL formation.

The next group contains the dust parameters and includes minimal and maximal grain sizes and the slope of the distribution  $n_{\text{dust}}$ . We let them vary in a wide range ex-

<sup>2</sup> <https://github.com/Semk0/EBL-model>

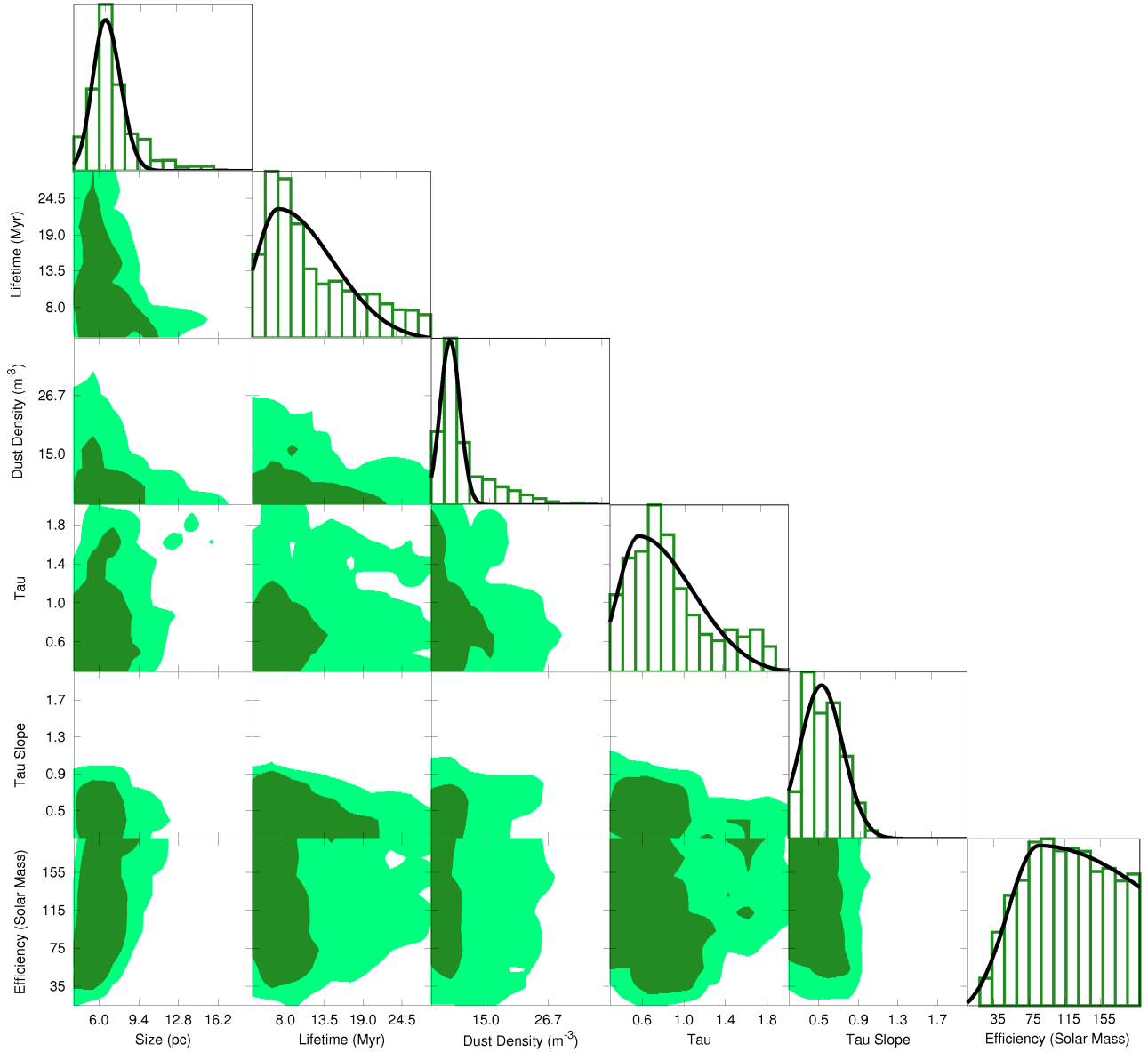


**Figure 2.** Distributions of the parameters of the clouds, including radius  $R_c$ , lifetime  $\eta_c$ , dust particle density  $n_d$ , optical depth at  $5500\text{\AA}$   $\tau_{\lambda_0}$ , optical depth slope  $n$  and cloud efficiency  $M_0$ .

cept for lower limit for the minimal grain sizes and upper limits for the maximal grain sizes which are  $10^{-3} \mu\text{ m}$  and  $1 \mu\text{ m}$  correspondingly. After the simulations we found that the grain sizes are constraint as:  $a_{\min} < 1.75 \cdot 10^{-3} \mu\text{ m}$  and  $a_{\max} < 22.8 \cdot 10^{-3} \mu\text{ m}$ . This is due to the higher emissivity of the bigger grains and thus greater contribution to the EBL. The slope of the distribution  $n_{\text{dust}}$  should be more than 3.83. The result may be expected at the large grains contribute more and their amount should be limited.

The third group collects all the parameters of the clouds, see Figure 2. Basically, the properties of the molec-

ular clouds are known from the observations of the Milky Way, for more details see, for instance, Murray (2011). Observations shows that the radii of the clouds lie in the range from 1 pc to 35 pc with the largest reach a size of 100 pc. The lifetimes of the clouds with the mean mass are  $17 \pm 4$  Myr Murray (2011). The following values are obtained from the MC for radius  $R_c = 6.1^{+1.4}_{-1.2}$  pc and lifetime  $\eta_c = 6.0^{+8.5}_{-3.6}$  Myr. These are in a good agreement with the experimental estimates. The relatively small value of the cloud radius may be reconciled with the observed larger clouds if we allow the large clouds to be inhomogeneous and divided into

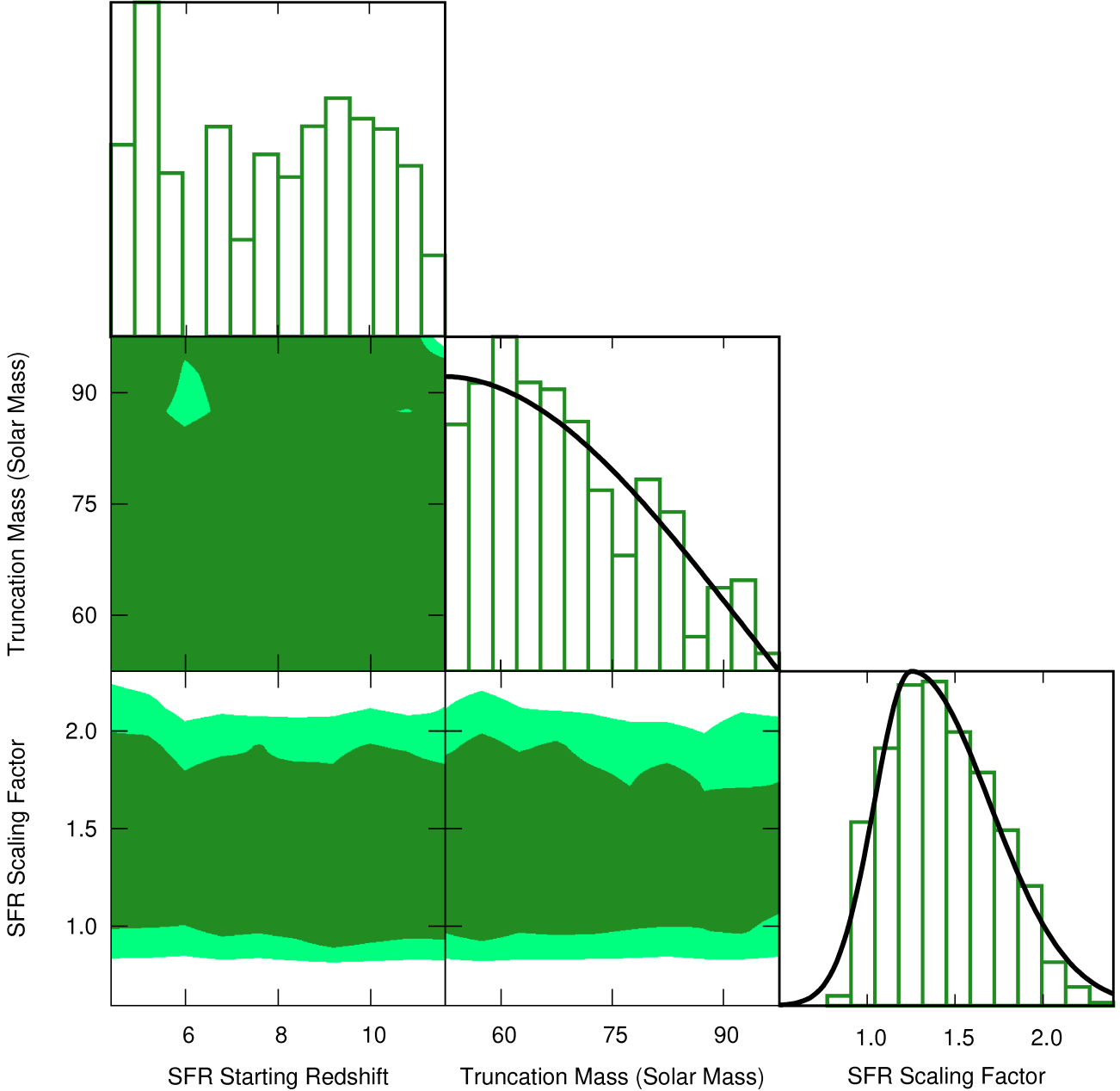


**Figure 3.** Distributions of the global parameters of star formation, including redshift at which star formation began  $z_i$ , IMF truncation mass  $m_{\max}$  and SFR scaling factor  $C_{\text{sfr}}$

the separate region of star formation. The dust particle density  $n_d$  can't be measured directly but may be derived from the mass of the cloud. One may derive the star formation efficiency  $\epsilon = 0.035$  which is defined as the ratio between the mass of the newborn stars in the cloud and the whole mass of the cloud. The calculation uses common assumption that the gas to dust ratio is 100. The value of  $\epsilon$  is in line with the modern observations Murray (2011).

The last group contains the global parameters of the Universe, see Figure 3. It includes the redshift of the beginning of the star formation, the mass of the star at which

IMF is truncated and scaling factor for the star formation rate. We obtained that the EBL does not depend on the epochs with the redshift  $4 < z < 10$ . Truncation mass is the maximal mass of the star in our model. We obtain that the smaller truncation masses are more probable than the bigger ones. The reasoning for this result is that the massive stars are too hot and thus overheat the dust. Finally, the star formation rate scaling factor is well constrained and at  $1-\sigma$  is  $1.25^{+0.44}_{-0.24}$ .

In the calculations above the results of CIBER and ESO VLT/FOR were used as the upper limits 3. It is practical

to know how the conclusions of the present paper change if these results are interpreted as the direct measurements. For this purpose a separate Markov Chain was constructed. The account of double-sided CIBER and ESO VLT/FOR gives the higher value of star formation rate  $C_{\text{sfr}} = 1.76^{+0.14}_{-0.13}$  and lower values of the radius and lifetime of the clouds  $R_c < 3.7 \pm 2.0$ ,  $\eta_c < 3.1 \pm 2.2$ .

## 5 CONCLUSION

We present the new flexible model of the EBL which is defined as a function of the astrophysical parameters. It was shown, that the spectrum based on the common values of these parameters lies in the experimentally admissible range and is in a good agreement with the models presented in literature. Further analysis was devoted to study the spectrum dependence on these parameters and set bounds for each of them. With the help of the Markov Chain Monte Carlo method we explored the parameter space and set up constraints on the star formation rate and parameters of the molecular clouds. Specifically, we have obtained the estimate of the IMF slope parameter  $a_{\text{imf}} = 2.29^{+0.15}_{-0.24}$ . Moreover, assuming the shape of the SFR from Gilmore et al. (2012) we obtain that the SFR scaling factor lies in the range from 1.01 to 1.69 at 68% C.L. The latter implies that the models with the overall decrease of the EBL intensity are constrained with the observational data.

## ACKNOWLEDGEMENTS

The authors are indebted to Maxim Pshirkov, Dmitry Semikoz, Sergey Troitsky and Valery Rubakov for inspiring discussions. This work has been supported by the Russian Science Foundation grant 14-22-00161. The numerical part of the work is performed at the cluster of the Theoretical Division of INR RAS. A.K. is supported by the fellowship of Basis Foundation.

## REFERENCES

### References

Ade P. A. R., et al., 2016, *Astron. Astrophys.*, 594, A13  
 Andrews S. K., Driver S. P., Davies L. J., Lagos C. d. P., Robotham A. S. G., 2017, [10.1093/mnras/stx2843](https://arxiv.org/abs/10.1093/mnras/stx2843)  
 Bernstein R. A., 2007, *The Astrophysical Journal*, 666, 663  
 Berta S., et al., 2010, *A&A*, 518, L30  
 Bethermin M., Dole H., Beelen A., Aussel H., 2010, *Astron. Astrophys.*, 512, A78  
 Béthermin M., et al., 2012, *A&A*, 542, A58  
 Calzetti D., Armus L., Bohlin R. C., Kinney A. L., Koornneef J., Storchi-Bergmann T., 2000, *Astrophys. J.*, 533, 682  
 Cambresy L., Reach W. T., Beichman C. A., Jarrett T. H., 2001, *Astrophys. J.*, 555, 563  
 Chabrier G., 2003, *Publ. Astron. Soc. Pac.*, 115, 763  
 Charlot S., Fall S. M., 2000, *ApJ*, 539, 718  
 Chary R.-R., et al., 2004, *Astrophys. J. Suppl.*, 154, 80  
 De Angelis A., Roncadelli M., Mansutti O., 2007, *Phys. Rev.*, D76, 121301  
 Devlin M. J., 2009, *Nature*, 458, 737  
 Dole H., et al., 2006, *Astron. Astrophys.*, 451, 417

Dominguez A., et al., 2011, *Mon. Not. Roy. Astron. Soc.*, 410, 2556  
 Dzhatdov T. A., Khalikov E. V., Kircheva A. P., Lyukshin A. A., 2017, *Astron. Astrophys.*, 603, A59  
 Essey W., Kusenko A., 2010, *Astroparticle Physics*, 33, 81  
 Fairbairn M., Rashba T., Troitsky S. V., 2011, *Phys. Rev.*, D84, 125019  
 Fazio G. G., et al., 2004, *Astrophys. J. Suppl.*, 154, 39  
 Finke J. D., Razzaque S., Dermer C. D., 2010, *Astrophys. J.*, 712, 238  
 Fixsen D. J., Dwek E., Mather J. C., Bennett C. L., Shafer R. A., 1998, *Astrophys. J.*, 508, 123  
 Franceschini A., Rodighiero G., 2017, *Astron. Astrophys.*, 603, A34  
 Franceschini A., Aussel H., Cesarsky C. J., Elbaz D., Fadda D., 2001, *Astron. Astrophys.*, 378, 1  
 Franceschini A., Rodighiero G., Vaccari M., 2008, *Astron. Astrophys.*, 487, 837  
 Frayer D. T., et al., 2006, *Astrophys. J.*, 647, L9  
 Gilmore R. C., Somerville R. S., Primack J. R., Dominguez A., 2012, *Mon. Not. Roy. Astron. Soc.*, 422, 3189  
 Gorjian V., Wright E. L., Chary R. R., 1999, Submitted to: *Astrophys. J.*  
 Horns D., Meyer M., 2012, *JCAP*, 1202, 033  
 Hurley J. R., Pols O. R., Tout C. A., 2000, *Mon. Not. Roy. Astron. Soc.*, 315, 543  
 Keenan R. C., Barger A. J., Cowie L. L., Wang W.-H., 2010, *Astrophys. J.*, 723, 40  
 Kneiske T. M., Mannheim K., Hartmann D. H., 2002, *Astron. Astrophys.*, 386, 1  
 Kneiske T. M., Bretz T., Mannheim K., Hartmann D. H., 2004, *Astron. Astrophys.*, 413, 807  
 Krugel E., 2003, *The Physics of Interstellar Dust*, 1 edn. Institute of Physics Publishing  
 Levenson L. R., Wright E. L., 2008, *Astrophys. J.*, 683, 585  
 Levenson L. R., Wright E. L., Johnson B. D., 2007, *Astrophys. J.*, 666, 34  
 Madau P., Pozzetti L., 2000, *Mon. Not. Roy. Astron. Soc.*, 312, L9  
 Madau P., Pozzetti L., Dickinson M., 1998, *Astrophys. J.*, 498, 106  
 Martinez-Galarza J. R., Kamp I., Su K. Y. L., Gaspar A., Rieke G., Mamajek E. E., 2009, *Astrophys. J.*, 694, 165  
 Matsuoka Y., Ienaka N., Kawara K., Oyabu S., 2011, *ApJ*, 736, 119  
 Matsuura S., et al., 2011, *ApJ*, 737, 2  
 Matsuura S., et al., 2017, *Astrophys. J.*, 839, 7  
 Mattila K., Väisänen P., Lehtinen K., von Appen-Schnur G., Leinert C., 2017, *MNRAS*, 470, 2152  
 Murray N., 2011, *Astrophys. J.*, 729, 133  
 Nikishov A., 1962, *Sov. Phys. JETP*, 14, 393  
 Pei Y. C., Fall S. M., Hauser M. G., 1999, *ApJ*, 522, 604  
 Primack J. R., Bullock J. S., Somerville R. S., MacMinn D., 1999, *Astropart. Phys.*, 11, 93  
 Rowan-Robinson M., 2001, *Astrophys. J.*, 549, 745  
 Rubtsov G. I., Troitsky S. V., 2014, *JETP Lett.*, 100, 355  
 Schlegel D. J., Finkbeiner D. P., Davis M., 1998, *Astrophys. J.*, 500, 525  
 Simet M., Hooper D., Serpico P. D., 2008, *Phys. Rev.*, D77, 063001  
 Stecker F. W., Scully S. T., Malkan M. A., 2016, *Astrophys. J.*, 827, 6  
 Troitsky S. V., 2017, *JETP Lett.*, 105, 55  
 Wright E. L., 2004, *New Astron. Rev.*, 48, 465  
 Xu C. K., et al., 2005, *Astrophys. J.*, 619, L11



**Table 1.** Mean values and  $1\text{-}\sigma$  C.L. for the MCMC variable parameters in comparison with the value, presented in literature. Dash in MCMC column means that the model does not depend on this parameter.

Parameter name	Symbol	MCMC	literature
IMF Parameter ( $M_{\odot}$ )	$m_0$	-	$0.079^{+0.021}_{-0.016}$ Chabrier (2003)
IMF Parameter	$D$	-	$0.69^{+0.05}_{-0.01}$ Chabrier (2003)
IMF Parameter	$a_{\text{imf}}$	$2.29^{+0.15}_{-0.24}$	$2.3 \pm 0.3$ Chabrier (2003)
Dust Particle Minimal Size ( $\mu\text{m}$ )	$a_{\text{min}}$	$< 1.75 \cdot 10^{-3}$	-
Dust Particle Maximal Size ( $\mu\text{m}$ )	$a_{\text{max}}$	$< 22.8 \cdot 10^{-3}$	-
Dust Distribution Slope	$n_{\text{dust}}$	$> 3.83$	$\sim 3.5$
Radius of the Cloud (pc)	$R_c$	$6.1^{+1.4}_{-1.2}$	2.5-100 Murray (2011)
Lifetime of the Cloud (Myr)	$\eta_c$	$6.0^{+8.5}_{-3.6}$	$\sim 10$ Murray (2011)
Dust Particle Density ( $m^{-3}$ )	$n_d$	$6.9 \pm 2.0$	$\sim 10$ Murray (2011)
Optical Depth at $5500 \text{ \AA}$	$\tau_{\lambda_0}$	$0.59^{+0.57}_{-0.21}$	$\sim 1$ Charlot & Fall (2000)
Optical Depth Slope	$n$	$0.47 \pm 0.24$	$\sim 0.7$ Charlot & Fall (2000)
Cloud Efficiency ( $M_{\odot}$ )	$M_0$	$85^{+152}_{-36}$	-
Redshift of the beginning of the star formation	$z_i$	-	$\sim 8$ Gilmore et al. (2012)
IMF Truncation Mass ( $M_{\odot}$ )	$m_{\text{max}}$	$< 84$	$\sim 100$
SFR scaling factor	$C_{\text{sfr}}$	$1.25^{+0.44}_{-0.24}$	$\sim 1$

**Table 2.** EBL lower limits used in this paper.

$\lambda$ ( $\mu\text{m}$ )	Lower Limits (nW/m <sup>2</sup> /sr)	Experiment
0.153	$1.03 \pm 0.15$	Galex Xu et al. (2005)
0.231	$2.25 \pm 0.32$	Galex Xu et al. (2005)
0.36	$2.87^{+0.58}_{-0.47}$	HDF Madau & Pozzetti (2000)
0.45	$4.57^{+0.73}_{-0.47}$	HDF Madau & Pozzetti (2000)
0.67	$6.74^{+1.25}_{-0.94}$	HDF Madau & Pozzetti (2000)
0.81	$8.04^{+1.62}_{-0.92}$	HDF Madau & Pozzetti (2000)
1.1	$9.71^{+3.0}_{-1.9}$	HDF Madau & Pozzetti (2000)
1.6	$9.02^{+2.62}_{-1.68}$	HDF Madau & Pozzetti (2000)
2.2	$7.92^{+2.04}_{-1.21}$	HDF Madau & Pozzetti (2000)
1.25	$11.7 \pm 2.6$	Subaru Keenan et al. (2010)
1.6	$11.5 \pm 1.5$	Subaru Keenan et al. (2010)
2.12	$10.0 \pm 0.8$	Subaru Keenan et al. (2010)
3.6	$5.4 \pm 1.4$	Spitzer/IRAC Fazio et al. (2004)
4.5	$3.5 \pm 0.9$	Spitzer/IRAC Fazio et al. (2004)
5.8	$3.6 \pm 0.9$	Spitzer/IRAC Fazio et al. (2004)
8.0	$2.6 \pm 0.7$	Spitzer/IRAC Fazio et al. (2004)
24	$2.29 \pm 0.09$	Spitzer/MIPS Bethermin et al. (2010)
70	$5.4 \pm 0.4$	Spitzer/MIPS Bethermin et al. (2010)
70	$7.4 \pm 1.9$	Spitzer/MIPS Frayer et al. (2006)
24	$2.0 \pm 0.2$	Spitzer/MIPS Chary et al. (2004)
70	$7.1 \pm 1.0$	Spitzer/MIPS Dole et al. (2006)
160	$13.4 \pm 1.7$	Spitzer/MIPS Dole et al. (2006)
100	$6.33 \pm 1.67$	Herschel/PACS Berta et al. (2010)
160	$6.58 \pm 1.62$	Herschel/PACS Berta et al. (2010)
250	$8.5 \pm 0.6$	BLAST Devlin (2009)
350	$4.8 \pm 0.3$	BLAST Devlin (2009)
500	$2.2 \pm 0.2$	BLAST Devlin (2009)
250	$7.4 \pm 1.42$	Herschel/SPIRE Béthermin et al. (2012)
350	$4.5 \pm 0.9$	Herschel/SPIRE Béthermin et al. (2012)
500	$1.54 \pm 0.34$	Herschel/SPIRE Béthermin et al. (2012)

## APPENDIX A

The numerical implementation of model from Section 2 is available at <https://github.com/SemkO/EBL-model>. There are two possible scenarios of using the code. First, the EBL spectrum may be constructed with the help of `spec.cpp` module. The parameters of the EBL are defined in the `in/param.txt` file. One may fine the full description of the parameters in the `spec.cpp` file. The second usage scenario is the optimization of the parameters for the specific EBL constraints. It is assumed that the data point are separated

into the three categories: upper limits, lower limits and direct measurements. The program read these points from the following files `in/upper_limits.txt`, `in/lower_limits.txt`, `in/direct.txt`. The make command compiles the code and starts optimization.

This paper has been typeset from a  $\text{\TeX}/\text{\LaTeX}$  file prepared by the author.

**Table 3.** EBL upper limits used in this paper.

$\lambda$ ( $\mu\text{m}$ )	Upper Limits ( $\text{nW}/\text{m}^2/\text{sr}$ )	Experiment
0.4	$11.6 \pm 1.7$	ESO VLT/FORSE <a href="#">Mattila et al. (2017)</a>
0.52	$23.4 \pm 4.7$	ESO VLT/FORSE <a href="#">Mattila et al. (2017)</a>
1.25	$21 \pm 15$	COBE/DIRBE <a href="#">Levenson et al. (2007)</a>
2.2	$20 \pm 6$	COBE/DIRBE <a href="#">Levenson et al. (2007)</a>
3.5	$13.3 \pm 2.8$	COBE/DIRBE <a href="#">Levenson et al. (2007)</a>
1.25	$54 \pm 16.8$	COBE/DIRBE <a href="#">Cambresy et al. (2001)</a>
2.2	$27.8 \pm 6.7$	COBE/DIRBE <a href="#">Cambresy et al. (2001)</a>
1.4	$28.7^{+5.1}_{-3.3}$	CIBER <a href="#">Matsuura et al. (2017)</a>
3.6	$9.0^{+1.7}_{-0.9}$	COBE/DIRBE <a href="#">Levenson &amp; Wright (2008)</a>
2.2	$22.4 \pm 6.0$	COBE/DIRBE <a href="#">Gorjian et al. (1999)</a>
3.5	$11.0 \pm 3.3$	COBE/DIRBE <a href="#">Gorjian et al. (1999)</a>
65	$12.5 \pm 9.3$	Akari <a href="#">Matsuura et al. (2011)</a>
90	$22.3 \pm 5.0$	Akari <a href="#">Matsuura et al. (2011)</a>
140	$20.1 \pm 3.6$	Akari <a href="#">Matsuura et al. (2011)</a>
160	$13.7 \pm 4.0$	Akari <a href="#">Matsuura et al. (2011)</a>
140	$12.6 \pm 6.0$	COBE/FIRAS <a href="#">Fixsen et al. (1998)</a>
160	$13.7 \pm 6.1$	COBE/FIRAS <a href="#">Fixsen et al. (1998)</a>
140	$32 \pm 13$	COBE/DIRBE <a href="#">Schlegel et al. (1998)</a>
240	$17 \pm 4$	COBE/DIRBE <a href="#">Schlegel et al. (1998)</a>
100	$12.5 \pm 5.0$	COBE/DIRBE <a href="#">Wright (2004)</a>
140	$22 \pm 7$	COBE/DIRBE <a href="#">Wright (2004)</a>
240	$13.0 \pm 2.5$	COBE/DIRBE <a href="#">Wright (2004)</a>

**Table 4.** Direct measurements of the EBL used in this paper.

$\lambda$ ( $\mu\text{m}$ )	Direct Measurements ( $\text{nW}/\text{m}^2/\text{sr}$ )	Experiment
0.44	$7.9 \pm 4.0$	Pioneer 10/11 <a href="#">Matsuoka et al. (2011)</a>
0.64	$7.7 \pm 5.8$	Pioneer 10/11 <a href="#">Matsuoka et al. (2011)</a>
240	$10.9 \pm 4.3$	COBE/FIRAS <a href="#">Fixsen et al. (1998)</a>
250	$10.3 \pm 4.0$	COBE/FIRAS <a href="#">Fixsen et al. (1998)</a>
350	$5.6 \pm 2.1$	COBE/FIRAS <a href="#">Fixsen et al. (1998)</a>
500	$2.4 \pm 0.9$	COBE/FIRAS <a href="#">Fixsen et al. (1998)</a>
850	$0.5 \pm 0.21$	COBE/FIRAS <a href="#">Fixsen et al. (1998)</a>